Improved Antibacterial Activity by Incorporation of Silver Sulfadiazine on Nanoporous Cu-BTC Metal-Organic-Framework

Sajjad Soltani

Kamran Akhbari (kmrn.akhbari@gmail.com)

College of Science https://orcid.org/0000-0002-4574-683X

Anukorn Phuruangrat

Research Article

Keywords: MOF, Silver sulfadiazine, Cu-BTC, Antibacterial activity, Synergistic effect, Nanoporous

Posted Date: March 14th, 2022

DOI: https://doi.org/10.21203/rs.3.rs-1436081/v1

Abstract

Silver sulfadiazine (SSD) as an antibacterial agent is widely used in the topical treatment of wound infections. Metal-organic frameworks (MOFs) have also been considered in the field of drug delivery in recent years due to their attractive properties. In this work, in order to increase the antibacterial efficiency, the Cu-BTC MOF was used as a platform for the incorporation of silver sulfadiazine. Physical characterization of compounds was performed using FT-IR, PXRD, SEM, TEM, EDX-mapping, N_2 adsorption-desorption and TGA techniques. The performance of the compounds against *Staphylococcus aureus* and *Escherichia coli* bacterium was assessed by agar well diffusion and plate colony count bioassays. SSD loading on the Cu-BTC MOF resulted in a synergistic effect in antibacterial activity.

1. Introduction

The emergence and outbreak of the pandemic COVID-19, which according to the report of the World Health Organization (WHO) has killed more than 5 million worldwide people by the end of 2021, has shown that infectious diseases can be serious threats to the human generation. Infectious diseases have irreparable consequences on the social and economic affairs of countries and challenge the health care system [1, 2]. It is necessary to implement basic actions to minimize the problems. One of the performed actions is the research and development of substances that can eliminate pathogens. In this regard, various organic, inorganic, and organic-inorganic hybrids compounds have been introduced [3–5]. The use of silver has been common since ancient times, and today, silver-based compounds are still considered by researchers in the combat against various infectious agents due to their broad-spectrum antibacterial properties [6, 7]. Burn injuries are costly due to the relatively long treatment period, and unfortunately, lead to many deaths each year [8, 9]. Burn wounds can become infected as a result of contact with pathogens, which can delay the healing of the skin due to the formation of skin lesions and cause side effects [10, 11]. So far, various antibacterial agents have been studied to treat burn infections. One of the well-known silver compounds for healing infectious wound burns is silver sulfadiazine, which is used topically in the experimental and clinical treatment of second and third-degree vulnerable infection [12, 13], and delivered in the form of 1% commercial creams or aqueous suspension [14]. In the silver sulfadiazine polymeric structure, there is a coordination bond between silver and sulfadiazine, and its antibacterial properties depend on the release of silver ions at the site of infection [15]. In order to improve the antibacterial performance, enhancement of the solubility, prevented the aggregation, optimum drug availability, controlling release, reduction of posing problem and allergic reactions of silver ions in silver sulfadiazine [13, 15–19], efforts are being made to achieve systems that stabilize it on other materials. This strategy can provide opportunities to perform topical treatment with a targeted release of the loaded agent [14]. In this regard, the loading of sulfadiazine silver on various materials such as: (□) biodegradable polymers or co-polymer supports (polyvinyl alcohol, polyrotaxane, zein, polyacrylonitrile, chitosan)[20–24], (□) inorganic meso/nano-porous material carriers (MCM-41, SBA-15 mesoporous silica particles) [16, 25, 26], (□) collagen and amino acid base material [13, 27, 28], (□) solid lipid [29], and (□) composite or a mixture of them [30–34] have been investigated in various efficient approaches such as

wound dressing, film, creams, suspension, and gel formulations. MOFs are organic-inorganic hybrid compounds formed by the coordination of metal ions and organic ligands. Features such as high surface area, structural diversity, good physicochemical stability, biological degradation and compatibility, low toxicity, and the presence of cavities that can be hosts for various compounds make these compounds attractive materials in various applications [35, 36]. In recent years, the use of such structures for loading drugs and therapeutic compounds has been reported [37]. Cu-BTC (also known as HKUST-1) is one of the famous MOFs that has been synthesized from copper ions and 1,3,5-Benzenetricarboxylic acid ligand. The presence of copper ions, which along with silver are among the well-known metals with antibacterial properties [38], having holes with a suitable volume of 9Å×9Å and good chemical-thermal stability, has introduced it not only as an antibacterial agent but also as a carrier for drug molecule [39–42]. In this report, we decided to test the potential of using Cu-BTC MOF as a carrier for silver sulfadiazine, considering the capacities expressed for them. After characterization of the structure, antibacterial activities were evaluated by agar well diffusion and plate colony count bioassays.

2. Experimental

2.1. Materials Analysis methods

Analytical grade Cu-BTC precursors and solvents were all prepared from Merck Company. Silver sulfadiazine was donated from Sobhan Daru Pharmaceutical Company, Iran. The Fourier Transform Infrared spectra were recorded on a Bruker Tensor 27 infrared spectrophotometer, operating in the region from 400 to 4000 cm^{-1}. The powder X-ray diffraction (PXRD) patterns were measured using a Philips X'Pert Pro powder X-ray diffractometer in 2θ angle range of 5–80° at the stepwise scan of 0.02° at 0.1 $s{\cdot}step^{-1}$. The surface morphology of the samples was analyzed using JEOL JSM 5410LV scanning electron microscope (SEM). The particle size and morphology were determined using JEOL JEM-2011 transmission electron microscope (TEM). Elemental compositions of the samples were investigated via energy dispersive spectroscopy (EDX) X-ray (Tescan Mira 3). N_2 adsorption-desorption results were determined at 77 K using the Brunauer- Emmett-Teller (BET) theory (Quantachrome, QDS-MP-30). Thermogravimetric measurements were performed with a NETZSCH STA 449 F3 Jupiter thermal analysis system with a heating rate of 10°C min^{-1} in nitrogen flow. The loaded SSD was characterized by an inductively coupled plasma (ICP) atomic emission spectrometer (VISTA-MPX CCD).

2.2. Preparation of SSD@Cu-BTC

Cu-BTC synthesis was performed by reflux method according to the previous report [43]. The incorporation of silver was done by the post-synthesis method to achieve a molar ratio of 10:1 from copper to silver. For this purpose, 0.0643 g of silver sulfadiazine was first dispersed in a mixture of 125 mL of DI water and 125 mL of ethanol for 1 hour. The MOF (0.3629 g), which had previously been activated for 4 hours at 160°C, was added to the solution and stirred at room temperature for 12 h. Finally, after filtering and washing with excess water, the product was dried at 50°C in an oven.

2.3. Antibacterial efficiency study

The samples' antibacterial capacity was studied by agar well diffusion and plate colony count bioassays according to the protocol used in our previous papers [44]. For this purpose, the evaluation was performed against the growth of *Staphylococcus aureus* (ATCC-6538) and *Escherichia coli* (ATCC 25922) bacteria, as two routine Gram-positive and Gram-negative bacteria in wound infection. In the well diffusion assay, first, the surface of Mueller Hinton Agar plates is inoculated with a 0.5 McFarland concentration inoculum of the test microorganism. After culturing the microorganisms, 60 mL of the SSD@Cu-BTC suspensions with a 20000 µg/mL concentration were introduced into punched wells in the plates with a depth of 4 mm. In the case of SSD and Cu-BTC, concentrations of 2750 and 17250 µg/mL were prepared according to the results of ICP-OES. The plates were then incubated at 37°C for 24 h to obtain results in preventing bacterial growth. For the colony count method, inoculums of bacteria were inoculated to the sterile Muller Hinton Broth to obtain a solution with a concentration of 1×10^5 CFU/mL. Except for Blank (B), solutions of the samples were prepared at the same concentrations in the agar well diffusion method and then incubated at 37°C for specific times (30 m, 4 h, 10 h, 24 h) at 100 rpm. Aliquots of the solutions were surface cultured on plates containing sterile Trypticase Soy Agar and incubated at 37°C for 24 h. Then, the number of viable colonies was counted, and the percentage of reduction relative to the control was calculated.

3. Results And Discussion

3.1. Fourier transform infrared analysis (FT-IR)

Information on the coordination state of functional groups in the compounds and the type of interaction between SSD and Cu-BTC was analyzed by FT-IR spectroscopy (Fig. 1). In the SSD spectrum, the bands at 3389 and 3341 cm^{-1} are related to the symmetric and asymmetric stretching vibrations of the amine group, respectively [29]. The band at 1652 cm^{-1} is also related to the bending vibration of the NH_2 group [24]. The bands at 1412, 1502, 1152 and, 1590 cm^{-1} are attributed to the vibrations of the phenyl and pyrimidine groups [12]. The strong bands at 1126 and 1350 cm^{-1} are due to symmetric and asymmetric stretching vibrations in the SO_2 group and the band at 1230 cm^{-1} is attributed to the C-N bonds [45]. Other peaks in wavelengths below 1000 cm^{-1} are caused by various bending vibrations of C-H and S-O bonds [46]. In the Cu-BTC spectrum, the bands at 1337 and 1434 cm^{-1}, and bands at 1623 and 1579 cm^{-1} are attributed to symmetric and asymmetric stretching vibrations of the carboxylate group, respectively [47, 48]. Bands at 1502 and 1479 cm^{-1} are due to the vibrations of the aromatic C = C bonds. Broadband between 2700 and 3700 cm^{-1} is attributed to OH groups in water molecules [47, 48]. The SSD@Cu-BTC spectrum is an amalgamation of the spectra in SSD and Cu-BTC. Although most of the bands in the SSD spectrum are covered by the bands in the Cu-BTC spectrum, but as highlighted in Fig. 1, some of the SSD bands are well recognizable in the SSD@Cu-BTC spectrum. The lower value of SSD than Cu-BTC can also be a reason for its bands' lower intensity [24].

3.2. Powder X-ray diffraction (PXRD) study

The crystal structure of the compounds was studied using the PXRD. As shown in Fig. 2, the as-Cu-BTC diffraction pattern has three main peaks at 2-theta angles of 6.74, 9.52, and 11.66 and some other peaks with lower intensities that are in good agreement with the simulated diffraction pattern of Cu-BTC [49]. In the simulated diffraction pattern of SSD [50], the two main peaks can be detected at 2-theta angles of 8.76 and 10.2. As shown in Fig. 2, the characteristic peaks of SSD and Cu-BTC are prominently present in the loaded Cu-BTC diffraction pattern. Filling of MOF cavities can a reason for the decrease in peak intensity after loading [26]. The absence of a significant characteristic peak from another phase after loading is a reason for the purity of the loaded sample but the absence of a main peak at 2-theta angle of 6.74 and observed shifts of SSD peak at 2-theta angle of 8.76 to lower 2-theta angle confirmed that the crystalline structure of Cu-BTC was changed approximately in SSD@Cu-BTC. Thus SSD@Cu-BTC has new crystalline form which is similar to crystalline structure of SSD and Cu-BTC. From the intensity of the peaks, it is clear that after loading, SSD is still in its crystalline form.

3.3. Morphology and composition

The surface morphology and particle shape in the compounds were investigated by SEM and TEM images. Figure 3a shows the SEM image of Cu-BTC in the form of hills with a few microns in size made up of a collection of smaller pieces. According to Fig. 3b, it is clear that the Cu-BTC particles deformed into smaller cuboid components after the SSD loading process, which is consistent with that observed in the PXRD patterns. Some minor changes in the diffraction pattern can be the result of this morphological change. Because microscopic images did not provide information about the distribution of silver particles, TEM images were used to obtain more information. The TEM image (Fig. 3c) shows the same morphology as the SEM image for the loaded Cu-BTC. Magnifying electron image in Fig. 3d shows SSD particles in the form of spherical particles with the size of 5 to 20 nm that have a uniform distribution in the Cu-BTC framework. The dispersion of elements in the composition of the compounds was investigated using EDX-mapping (Fig. 4). The images prove the presence of silver particles and their uniform distribution along with other elements. The presence of nitrogen and sulfur as other SSD constituents indicates that silver is loaded on the Cu-BTC as part of the SSD structure and not as a separate phase.

3.4. N_2 gas adsorption measurements

N_2 gas adsorption measurements were performed at 77 K to determine the surface area and porosity volume. As-Cu-BTC has the pore volume and BET surface area of 0.60 $cm^3.g^{-1}$ and 1560 $m^2.g^{-1}$, respectively [43]. After loading, the pore volume and BET surface area were reduced to 0.11 $cm^3.g^{-1}$ and 27 $m^2.g^{-1}$, respectively. A significant decrease in these values indicates that a large amount of SSD particles are trapped inside the pores.

3.5. Thermal stability and the amount of SSD loaded

The response of the compounds to the applied heat was assessed by Thermogravimetric analysis (TGA). Cu-BTC and SSD@Cu-BTC thermographs are shown in Fig. 5. The Cu-BTC curve consists of two parts.

The first part up to about 300 ºC is due to the removal of non-coordinated and coordinated water molecules with a weight loss of 18.4%, and the next part up to 375 ºC is due to the decomposition of the MOF structure and loss of BTC ligand with a weight loss of 36.4%. Despite the similar behavior that is associated with the two weight loss, the SSD@Cu-BTC also has differences with the Cu-BTC. Removal of solvent molecules in the SSD@Cu-BTC up to 185 ºC is associated with irregularities. This behavior is affected by the presence of the SSD in the pores and on the surface of Cu-BTC, which interferes with the gradual removal of water molecules. Sudden weight loss in the second part of the curve also occurred at a lower temperature than Cu-BTC and at the temperature of 286 ºC. Considering the degradation temperature of the SSD (about 290 ºC) [51], it can be concluded this weight loss occurred due to the degradation of the drug before the decomposition of the MOF structure. With a weight loss of 29.1% to 356 ºC, the curve reaches an almost constant value. The distance between the ends of the Cu-BTC and SSD@Cu-BTC curves at 800 ° C is 13.3%, which indicates the amount of SSD loaded [22, 26, 34]. The amount of SSD loaded was also checked using ICP-OES analysis, and a value of 13.77% was obtained.

3.6. Bactericidal activity

First, the antibacterial capacity of the samples was examined in agar well diffusion bioassay by measuring the diameter of the inhibition zones, a halo around the wells in which the growth of microorganisms has stopped. *Escherichia coli* (E. coli) and *Staphylococcus aureus* (S. aureus) bacteria were selected as the two most common representatives of Gram-negative and Gram-positive pathogenic strains responsible for wound infection, respectively. The results are illustrated in Fig. 6 and summarized in Table 1. In this method, Cu-BTC did not have any activity on any of the bacteria, so according to the observed activity of SSD, the inhibition diameter created for SSD@Cu-BTC can be attributed to it. Against E. coli, the activity of SSD@Cu-BTC is significantly better, indicating an improved antibacterial activity of SSD after loading on Cu-BTC. The solubility of the compounds in the agar well diffusion method is limited. To solve this problem, plate colony count bioassay was used to gain a more accurate understanding of their function in conditions close to the biological conditions of the body. The reduction in the number of bacterial colonies for different times is shown in Fig. 7 and summarized in Table 2. In this method, SSD@Cu-BTC had a more tangible effect on two bacteria than SSD and Cu-BTC. It is clear that for SSD@Cu-BTC, the growth of bacteria was inhibited in a short time, and a reduction of 50% and 60% of the colony occurred for the S. aureus and E. coli strains within 30 m, respectively. The reduction in the number of colonies created by SSD@Cu-BTC after 4 h for E. coli has reached > 99% and no colony is seen after 10 h, which means complete death of the bacterium. In the case of S. aureus bacteria, although 99% of the colonies decreased after 4 h compared to the blank form, the growth did not stop completely for 24 h. Different susceptibility of two bacteria originated from their different cellular structures. The thinner cell wall of E. coli can be the cause of its greater weakness [52]. The occurrence of antibacterial activity in Cu-BTC shows its cooperation with SSD in SSD@Cu-BTC and a kind of synergistic effect has been created between them. In the case of Cu-BTC, the copper ions in its framework have been shown to be responsible for antibacterial activity [53]. In fact, the Cu-BTC instability in the aqueous medium over time causes the release of copper ions, which can have a multiplier effect on bacteria along with silver ions produced by SSD loaded on it. Copper and silver ions through the biological moieties

containing donor nitrogen, sulfur, and oxygen atom penetrate in the bacterial cell membrane, interfering with their biological functions and causing their death [54, 55].

Table 1
Zones of inhibitions against E. coli and S. aureus.

Compound	Zone of inhibition (mm)	
	E. coli	S. aureus
Cu-BTC	0	0
SSD	11	14
Cu-BTC@SSD	17	12

Table 2
Percentage reduction of bacterial colonies at different times

Compounds	Decreased number of E. coli colonies per time (%)			
	30 m	4 h	10 h	24 h
Cu-BTC	10	55	> 99.99	> 99.99
SSD	12	65	> 99.99	> 99.99
Cu-BTC@SSD	60	> 99	100	100
Blank	0	0	0	0
Compounds	Decreased number of S. aureus colonies per time (%)			
	30 m	4 h	10 h	24 h
Cu-BTC	5	40	90	> 99.99
SSD	5	45	95	> 99.99
Cu-BTC@SSD	50	99	> 99.99	> 99.99
Blank	0	0	0	0

4. Conclusion

In this work, the use of Cu-BTC as a platform for loading silver sulfadiazine antibacterial drug was investigated. Successful drug loading was demonstrated using FT-IR, PXRD and EDX-mapping. The adsorption of silver sulfadiazine particles has not been done through chemical interaction with Cu-BTC. TEM and EDX-mapping showed a uniform distribution of drug particles in the Cu-BTC structure. Due to the fact that Cu-BTC and SSD both have antibacterial properties, synergistic antibacterial activity was created after loading due to their simultaneous presence. E.coli was more sensitive to the compounds

due to the thinner cell wall. The results show that SSD@Cu-BTC can be considered as a promising antibacterial agent. However, clinical trials are needed to investigate its use in the treatment of wound infection.

Declarations

Acknowledgments

The authors consider it necessary to appreciate the financial support of the University of Tehran under Grant No. 01/1/389845 for this work.

Conflict of interest

The authors declare that they have no conflicts of interest with the contents of this article.

References

1. A. I. White. The Lancet. 395, 1250 (2020)
2. D.E. Bloom, D. Cadarette, Front. Immunol. **10**, 549 (2019)
3. S. Saidin, M.A. Jumat, N.A.A.M. Amin,A. S. S. Al Hammadi. Mater. Sci. Eng. C. 111382 (2020)
4. Q. Cheng, X. Guo, X. Hao, Z. Shi, S. Zhu, Z. Cui, ACS Appl. Mater. Interfaces **11**, 42607 (2019)
5. H.-C. Yang, J. Hou, V. Chen, Z.-K. Xu, J. Mater. Chem. A **4**, 9716 (2016)
6. G. Franci, A. Falanga, S. Galdiero, L. Palomba, M. Rai, G. Morelli, M. Galdiero. Molecules. **20**, 8856 (2015)
7. L. Rizzello, P. P. Pompa. Chem. Soc. Rev. **43**, 1501 (2014)
8. M. Bailey, H. Sagiraju, S. Mashreky, H. Alamgir. Burns. **45**, 957 (2019)
9. N.-A. Latifi, H. Karimi, S.A. Motevalian, ,M. Momeni. J. Burn Care Res. **38**, e900 (2017)
10. P. Jault, T. Leclerc, S. Jennes, J.P. Pirnay, Y.-A. Que, G. Resch, A.F. Rousseau, F. Ravat, H. Carsin, R. Le Floch. Lancet Infect. Dis. **19**, 35 (2019)
11. D. Church, S. Elsayed, O. Reid, B. Winston, R. Lindsay, Clin. Microbiol. Rev. **19**, 403 (2006)
12. G.S. El-Feky, S.T. El-Banna, G. El-Bahy, E. Abdelrazek, M. Kamal. Carbohydr. Polym. **177**, 194 (2017)
13. N. Shanmugasundaram, T. Uma, T. Ramyaa Lakshmi, M. Babu, J. Biomed. Mater. Res. Part. A **89**, 472 (2009)
14. P.M. Kumar, A. Ghosh, Eur. J. Pharm. Sci. **96**, 243 (2017)
15. F.L. Mi, Y.B. Wu, S.S. Shyu, J.Y. Schoung, Y.B. Huang, Y.H. Tsai, J. Y Hao J. Biomed. Mater. Res. Part. A **59**, 438 (2002)
16. Á Szegedi, M. Popova, K. Yoncheva, J. Makk, J. Mihály, P. Shestakova. J. Mater. Chem. B. **2**, 6283 (2014)

17. T. Luo, S. Shakya, P. Mittal, X. Ren, T. Guo, M.G. Bello, L. Wu, H. Li, W. Zhu, B. Regmi, Int. J. Pharm. **584**, 119407 (2020)
18. N. Joshi, N. Mishra, V.K. Rai, J. Pharm. Innov., 1 (2020)
19. Y. Ma, L. Xin, H. Tan, M. Fan, J. Li, Y. Jia, Z. Ling, Y. Chen, X. Hu. Mater. Sci. Eng. C. **81**, 522 (2017)
20. D. Gao, X. Zhou, Z. Gao, X. Shi, Z. Wang, Y. Wang, P. Zhang, J. Pharm. Sci. **107**, 2377 (2018)
21. S. Liu, C. Zhong, W. Wang, Y. Jia, L. Wang, L Ren. Polymers **10**, 190 (2018)
22. S. Ullah, M. Hashmi, M.Q. Khan, D. Kharaghani, Y. Saito, T. Yamamoto, I.S. Kim, RSC Adv. **9**, 268 (2019)
23. S. Ullah, M. Hashmi, D. Kharaghani, M.Q. Khan, Y. Saito, T. Yamamoto, J. Lee, I.S. Kim, Int. J. Nanomed. **14**, 2693 (2019)
24. W. Shao, J. Wu, S. Wang, M. Huang, X. Liu, R. Zhang. Carbohydr. Polym. **157**, 1963 (2017)
25. J.-K. Jo, A. El-Fiqi, J.-H. Lee, D.-A. Kim, H.-W. Kim, H.-H. Lee, Dent. Mater. **33**, e361 (2017)
26. S. Jangra, S. Devi, V.K. Tomer, V. Chhokar, S. Duhan, J. Asian Ceram. Soc. **4**, 282 (2016)
27. A.-R.C. Lee, H. Leem, J. Lee, K. C. Park. Biomaterials. **26**, 4670 (2005)
28. Y. Kuroyanagi, E. Kim, N. Shioya, J. Burn Care Rehabil **12**, 106 (1991)
29. C. Laura, S. Milena, B. Giovanna, B.M. Cristina, S. Giuseppina, B. Giampiero. J. Therm. Anal. Calorim. **111**, 2149 (2013)
30. P.Hissae Yassue-Cordeiro, C. Henrique Zandonai, B. Pereira Genesi, P. Santos Lopes, E. Sanchez-Lopez, M. Luisa Garcia, N. Regina Camargo, P. Fernandes-Machado, E.B. Severino, C. Souto, Ferreira da Silva. Pharmaceutics. **11**, 535 (2019)
31. F. Nejaddehbashi, M. Hashemitabar, V. Bayati, M. Abbaspour, E. Moghimipour, M. Orazizadeh. Artif. Organs. **43**, 413 (2019)
32. D.N. Heo, D.H. Yang, J.B. Lee, M.S. Bae, J.H. Kim, S.H. Moon, H.J. Chun, C.H. Kim, H.-N. Lim, J. Biomed. Nanotechnol **9**, 511 (2013) ,I. K. Kwon.
33. C. Aguzzi, G. Sandri, C. Bonferoni, P. Cerezo, S. Rossi, F. Ferrari, C. Caramella, C. Viseras, Colloids Surf. B **113**, 152 (2014)
34. M. Heo, S.J. Lee, D.N. Heo, D. Lee, H.-N. Lim, J.-H. Moon, I.K. Kwon, Appl. Surf. Sci. **432**, 308 (2018)
35. A.C. McKinlay, R.E. Morris, P. Horcajada, G. Férey, R. Gref, P. Couvreur, C. Serre. Angew. Chem., Int. Ed. **49**, 6260 (2010)
36. H. Cai, Y.-L. Huang, D. Li, Coord. Chem. Rev. **378**, 207 (2019)
37. L. Wang, M. Zheng, Z. Xie, J. Mater. Chem. B **6**, 707 (2018)
38. S. Soltani, K. Akhbari, J. White, Z. Anorg. Allg. Chem. (2020)
39. F.R.S. Lucena, L.C. de Araújo, M.d.D. Rodrigues, T.G. da Silva, V.R. Pereira, G.C. Militão, D.A. Fontes, P.J. Rolim-Neto, Biomed. Pharmacother **67**, 707 (2013) F. F. da Silva,S. C. Nascimento.
40. K. Singbumrung, K. Motina, P. Pisitsak, P. Chitichotpanya, S. Wongkasemjit, T. Inprasit. Fibers Polym. **19**, 1373 (2018)

41. S. Soltani, K. Akhbari. JBIC, J. Biol. Inorg. Chem., 1 (2021)
42. S. Soltani, K. Akhbari, A. Phuruangrat, Appl. Organomet. Chem., e6634 (2022)
43. M.A. Gotthardt, R. Schoch, S. Wolf, M. Bauer, W. Kleist, Dalton Trans. **44**, 2052 (2015)
44. S. Soltani, K. Akhbari, J. White CrystEngComm **23**, 7450 (2021)
45. W. Shao, H. Liu, X. Liu, S. Wang, J. Wu, R. Zhang, H. Min, M. Huang, Carbohydr. Polym. **132**, 351 (2015)
46. M. Rendošová, Z. Vargova, D. Sabolova, N. Imrichova, D. Hudecova, R. Gyepes, B. Lakatoš, K. Elefantova. J. Inorg. Biochem. **186**, 206 (2018)
47. X. Xia, W. Li, S. Li, J. Nanopart. Res. **21**, 1 (2019)
48. B. Zhang, J. Zhang, C. Liu, X. Sang, L. Peng, X. Ma, T. Wu, B. Han, G. Yang. RSC Adv. **5**, 37691 (2015)
49. S.S.-Y. Chui, S.M.-F. Lo, J.P. Charmant, A.G. Orpen, I. D. Williams. Science. **283**, 1148 (1999)
50. D.S. Cook, M.F. Turner. J. Chem. Soc. Perkin Trans. **2**, 1021 (1975)
51. S.V. Ghodekar, S. P. Chaudhari,M. Ratnaparakhi. Int. J. Pharm. Pharm. Sci. **4**, 305 (2012)
52. A. Mai-Prochnow, M. Clauson, J. Hong, A. B. Murphy. Sci. Rep. **6**, 1 (2016)
53. A.R. Abbasi, K. Akhbari, A Morsali Ultrason. Sonochem **19**, 846 (2012)
54. S.W. Jaros, M.F. t., C. Guedes da Silva, J. Król, M. Conceição, P. Oliveira, A.J. Smolenski, A.M. Pombeiro, Kirillov, Inorg. chem. **55**, 1486 (2016)
55. P. Makvandi, C.y. Wang, E.N. Zare, A. Borzacchiello, L. n. Niu,F. R. Tay. Adv. Funct. Mater. **30**, 1910021 (2020)

Figures

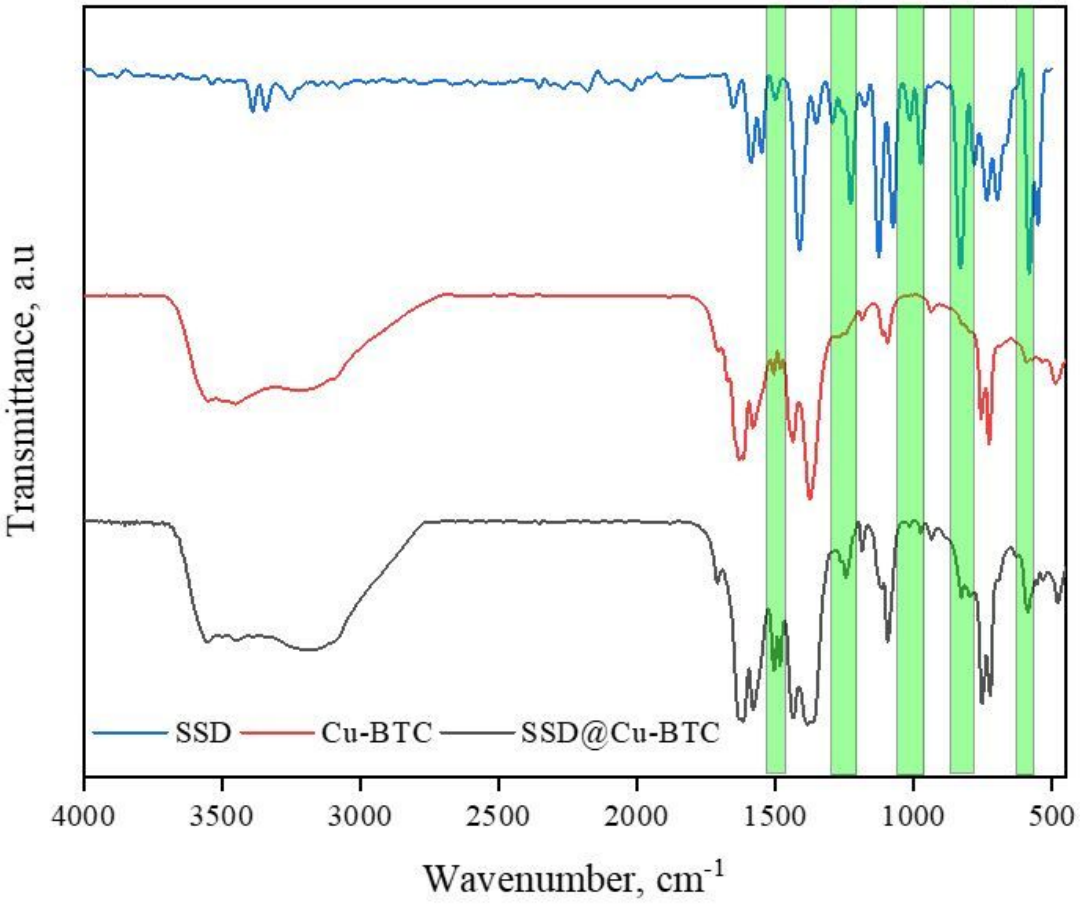

Figure 1

FT-IR spectra of compounds.

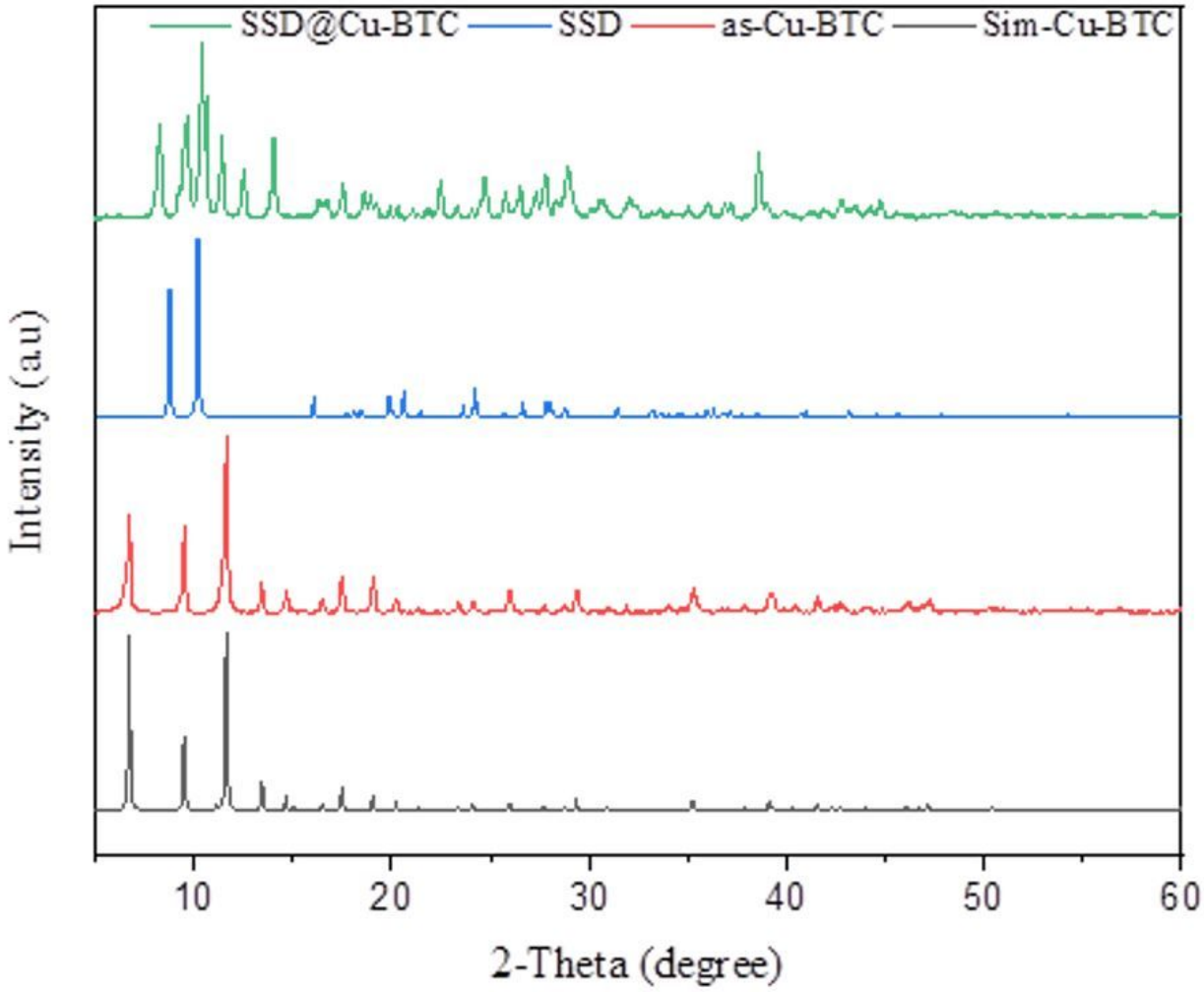

Figure 2

PXRD patterns of compounds.

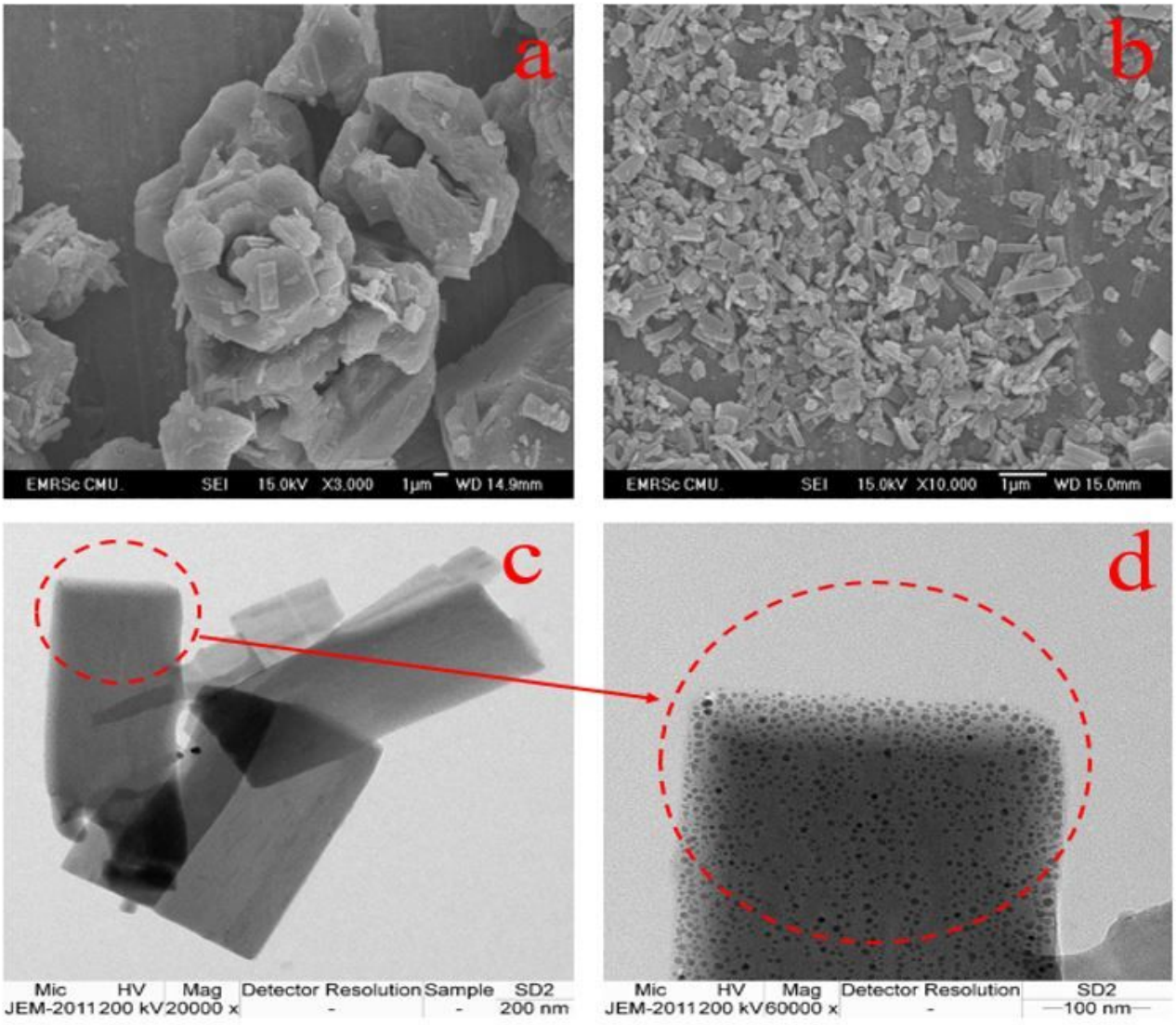

Figure 3

SEM images of Cu-BTC (a), SSD@Cu-BTC (b) and TEM image of SSD@Cu-BTC (c), magnified TEM image of SSD@Cu-BTC (d).

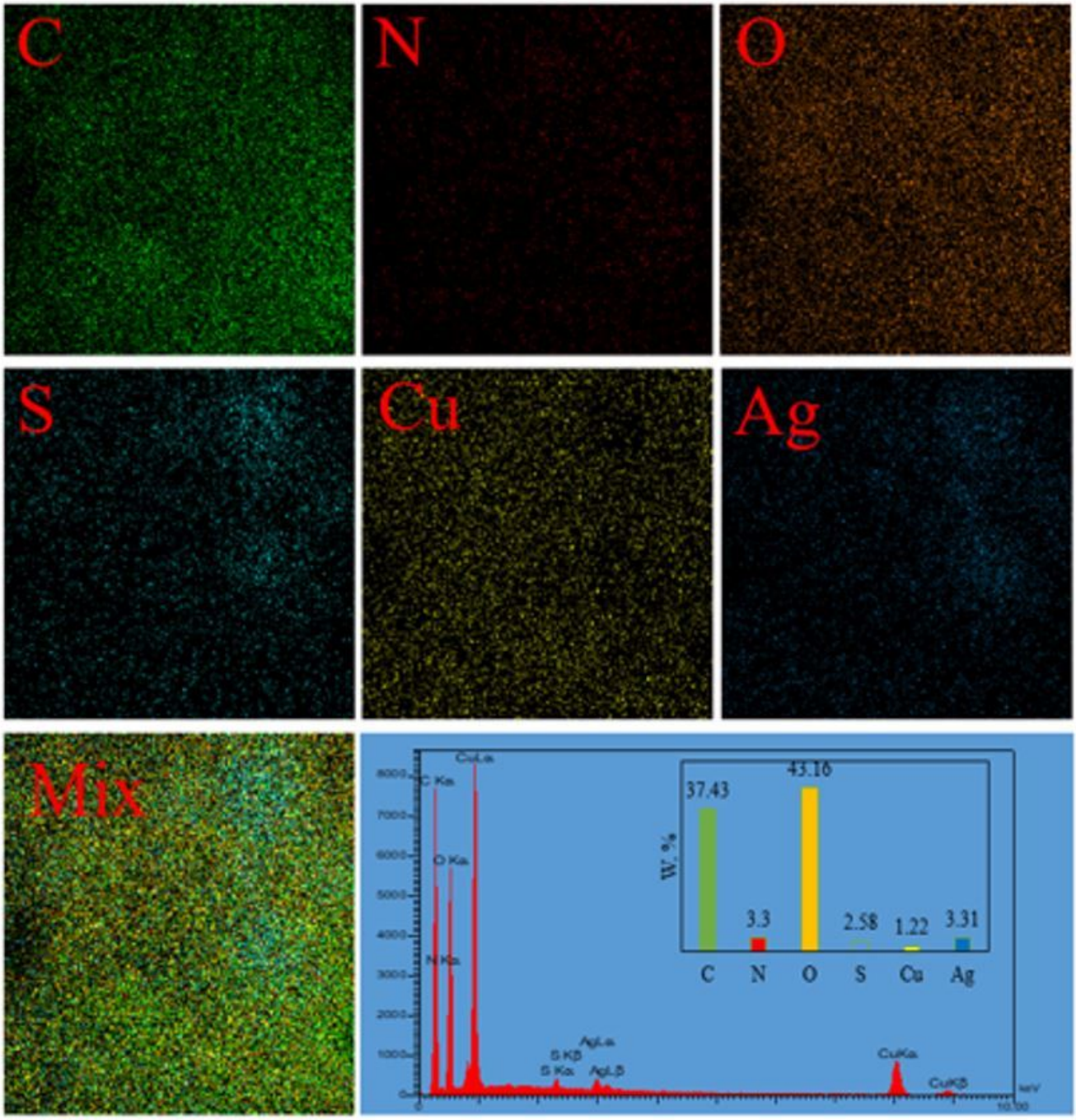

Figure 4

EDS-mapping and EDS spectrum of SSD@Cu-BTC.

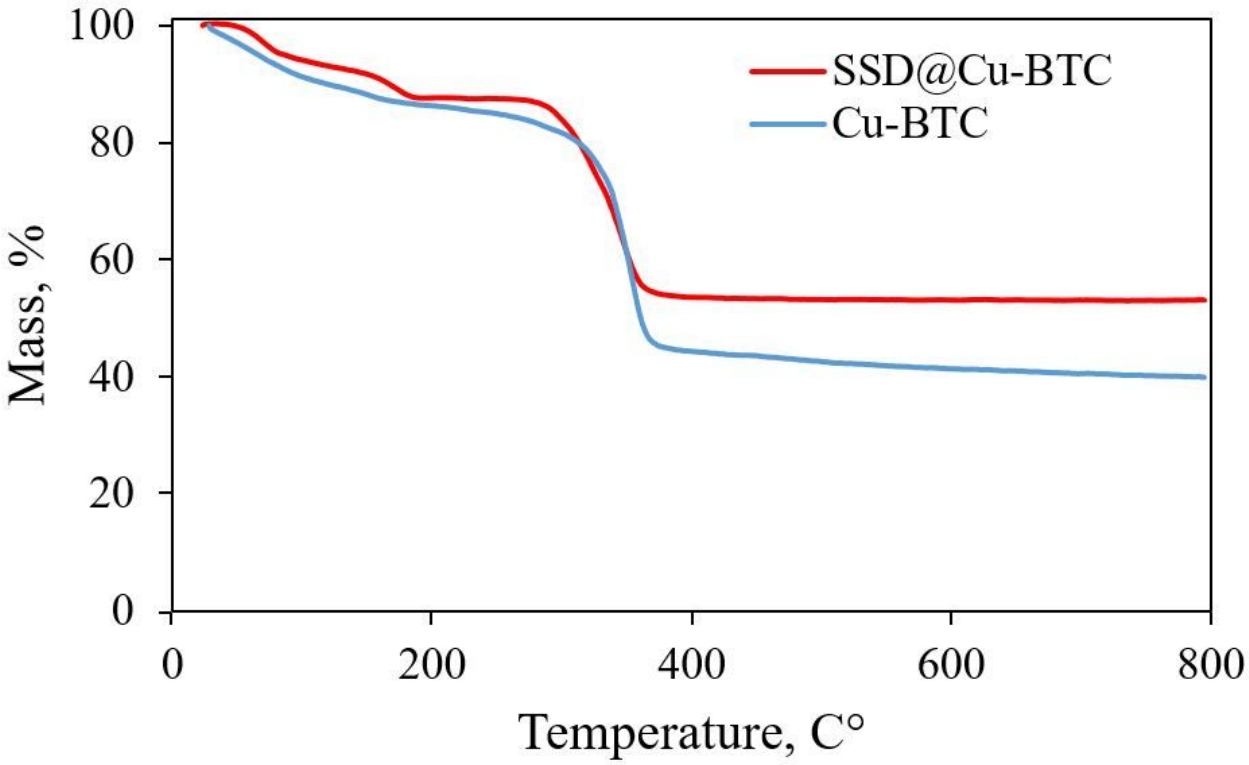

Figure 5

Thermogravimetric curves of Cu-BTC (blue) and SSD@Cu-BTC (red).

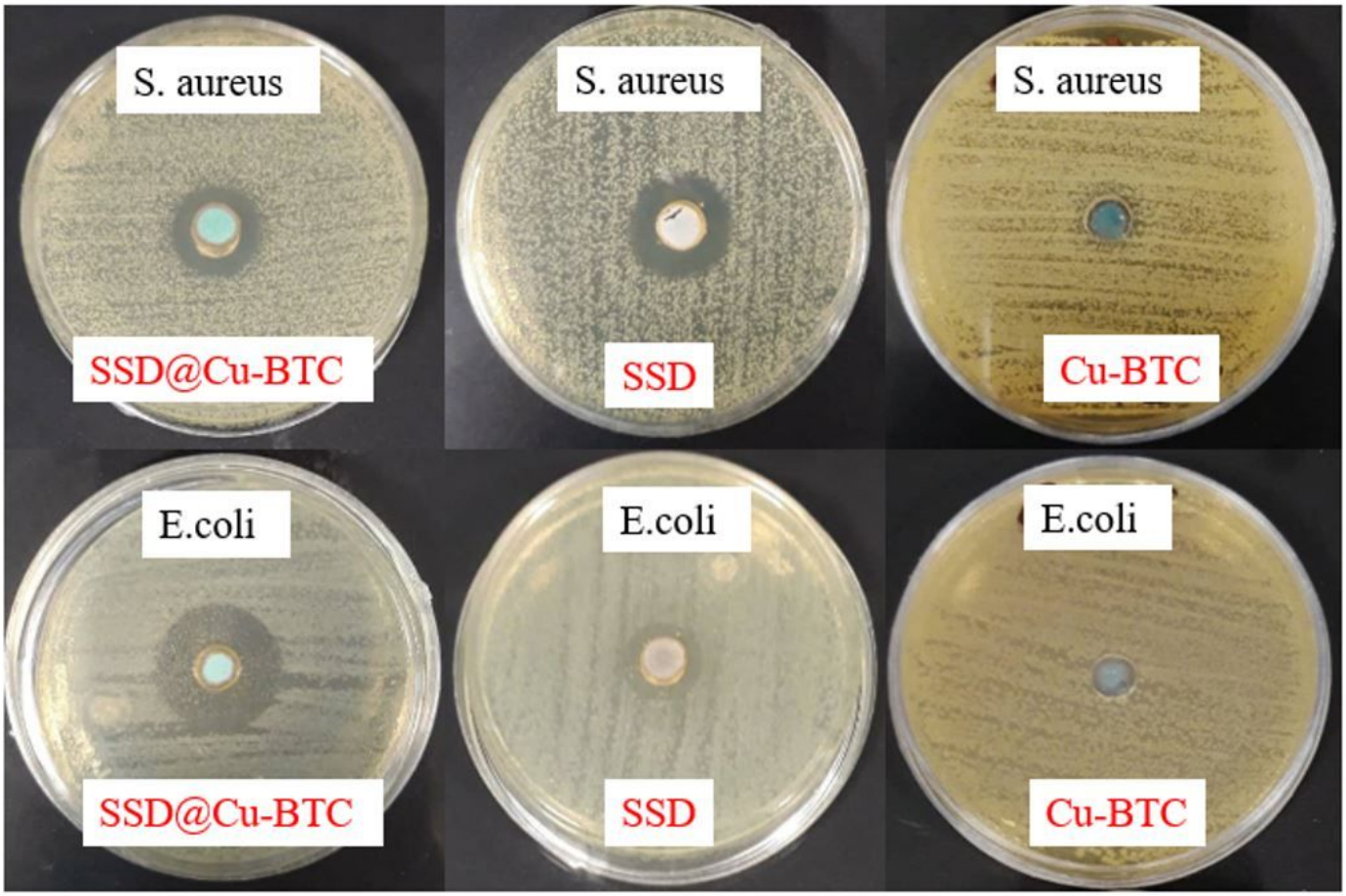

Figure 6

Zone of inhibition for compounds against E.coli and S.aureus strains.

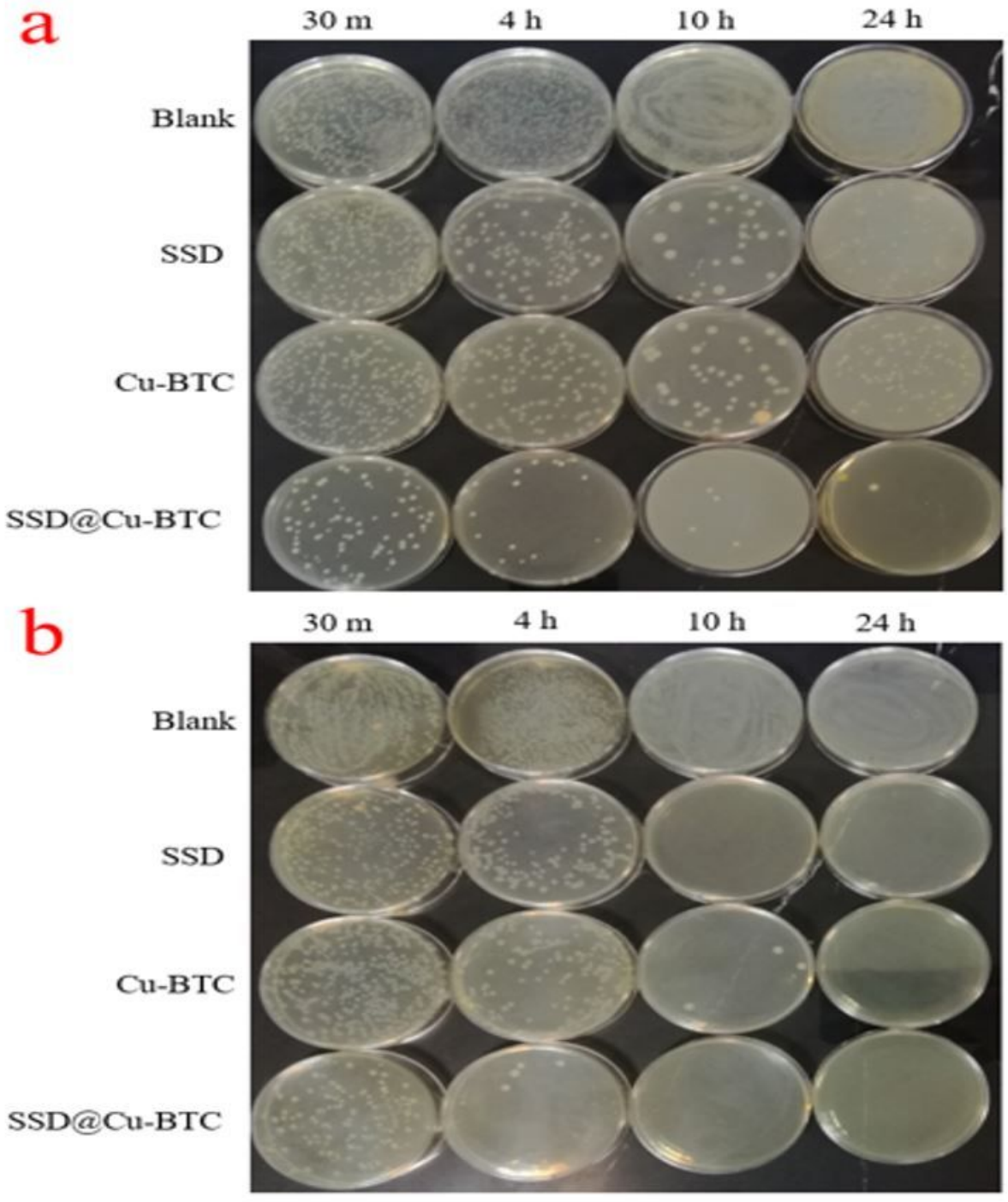

Figure 7

Bacterial colonies at different times against S.aureus (a) and E.coli (b) strains.